Yonsei Medical Journal
Vol. 44, No. 3, pp. 429-437, 2003

Pharmacokinetic Modeling of Phagocytic Activity of the Liver Using Superparamagnetic Iron Oxide Nanoparticles in Dynamic MR Imaging

Jae Boem Na[1], Jin-Suck Suh[2], Yong-Min Huh[2], Sung-Joon Kim[2], Seung-Hyung Kim[2], Seung-Whan Cha[2], and Sang-Hoon Lee[2]

[1]*Department of Radiology, Gyeongsang National University College of Medicine, Gyeongsangnam-do, Korea;*
[2]*Department of Radiology, Yonsei University College of Medicine, Research Institute of Radiological Science, Seoul, Korea.*

The purpose of this study was to determine whether phagocytic activity is measurable by dynamic superparamagnetic iron oxide-enhanced MR imaging. For these experiments on New Zealand White rabbits, which were randomly allocated to normal and silica treated groups, we performed a dynamic MR study and radioisotope study with Tc^{99m}-phytate. In this dynamic MR study, the ratio (Rv) of the distribution volumes of iron oxide (Vm/Ve) could be obtained by applying three-compartment model to the data obtained from the kidney and liver simultaneously. Changes in Rv caused by silica injection and by dosing superparamagnetic iron oxide, AMI-25, were evaluated. In the dynamic MR study using a Beagle dog model the input function could be calculated from data obtained from the hepatic artery and portal vein. Rv's reached maximum values at around 80 minutes after the AMI-25 injection. The Rv of the normal group was 5.06 ± 1.53 whereas the Rv of the silica treated group was 2.13 ± 1.20. The results were similar to tissue count data obtained by radioisope study. The Rv value was not dependent on the injected dose of AMI-25. The rate of transport constants (k1, k2, k3) could not be estimated using the 3 compartment model regardless of obtaining the input function. We conclude that Rv may be an quantitative index of decreased phagocytic activity in the liver as determined by dynamic superparamagnetic iron oxide-enhanced MRI.

Key Words: Superparamagnetic iron oxide, contrast agent, magnetic resonance imaging, liver, kupffer cell, phagocytes, compartment model, qualification

Received September 23, 2002
Accepted January 27, 2003

This work was supported by Korea Research Foundation Grant. (KRF-2000-041-F00261).

Reprint address: requests to Dr. Jin-Suck Suh, Department of Diagnostic Radiology, Yonsei University College of Medicine, 134 Shinchon-dong, Seodaemun-gu, Seoul 120-752, Korea. Tel: 82-2-361-5840, Fax: 82-2-393-3035, E-mail: jss@yumc.yonsei.ac.kr

INTRODUCTION

Iron oxide nanoparticles show a specific distribution in the liver, for they are phagocytosed from the blood by the reticulo-endothelial system and are deposited mainly in the Kupffer cells of the liver. Unlike gadolinium-DTPA (Gd-DTPA), iron oxide nanoparticles increase transverse relaxation and act as a negative contrast agent on T2-weighted images of the liver.[1-4] Moreover, the lowering of liver parenchymal signal intensity increases the detectability of hepatic tumors significantly.[5-8]

It is well known that relaxation rate changes ($\triangle R_2$) are proportional to the concentration of iron oxide, *in vivo* and *in vitro*,[1-3,6,9] and that iron oxide concentrations in a specific organ can be measured from signal intensity of magnetic resonance (MR) imaging, which make quantitative analysis and pharmacokinetic study possible. Many types of iron oxide nanoparticles have been developed and it is known that blood clearance by macrophages is dependent upon particle size. Polycrystalline particles such as AMI-25 (Advanced Magnetics, Cambridge, MA, USA) are rapidly cleared by Kupffer cells in the liver, whereas monocrystalline particles are cleared relatively slowly and the plasma half time ($T_{1/2}$) becomes longer.[9-11]

Pharmacokinetic modeling is widely used in radionuclide studies with single photon emission computed tomography (SPECT) and positron emission tomography (PET).[12-15] Many radionuclide studies have used direct blood sampling and

radioactivity measurements to determine the arterial input to concerned organs in a compartment model.[14,15] Transport rates (k1, k2, k3, k4) among the compartments may be determined using graphical analysis methods. Obtaining input function using this method involves invasive study.

Many studies using kinetic models in combination with graphical or other analytical methods have been used to analyze the time-$\triangle R_2$ curve. To estimate the transport rate between biological compartments, the input function of the system should be measured. These are 20% in the case of the hepatic artery and 80% for the portal vein. Because of this limitation, no attempts have been made to quantify the phagocytic activity by the application of the three-compartment model to dynamic MR study with iron oxide. This study was undertaken to determine whether phagocytic activity is measurable by using dynamic superparamagnetic iron oxide-enhanced MR imaging.

MATERIALS AND METHODS

Theory

Assumptions

(1) Hepatic sinusoidal blood iron oxide concentrations are the sum of hepatic and portal blood concentrations over time.

(2) $\triangle R_2(t)=-\ln[S(t)/S(0)]/T_E$, where S0 is the signal intensity of the pre-injection baseline and S(t) is that following injection at time t=0. $\triangle R_2$ is proportional to the concentration of iron oxide agent, *in vivo*.[9] $\triangle R_2$ in blood is approximately equal to $\triangle R_2$ in liver tissue.

(3) Tracer kinetics can be described by a three-compartment model consisting of an exchangeable tissue compartment plus a single compartment into which there is unidirectional flux (trapping), because the mechanism of iron oxide uptake to the Kupffer cell may be considered an irreversible process by receptor-mediated phagocytosis at least over the first 3 hours.

(4) The system obeys first order kinetics for transfer between compartments.[12]

(5) Tracer is on steady state.[12,13]

Pharmacokinetic Model

The kinetics of iron oxide can be described by a three-compartment model. After its transfer from plasma to interstitial space, iron oxide agent is phagocytosed by Kupffer cells. Therefore, the three-compartment model includes plasma, extracellular interstitial space and Kupffer cells (Fig. 1).

The total content of iron oxide agent per unit mass of liver tissue, Ci (the concentration of extravascular space including extracellular interstitial space and Kupffer cells), is equal to the sum of Ce and Cm. This derivative with respect to time, t, is

$$dCi/dt = dCe/dt + dCm/dt \quad (1)$$

where *dCE/dt* is equal to the difference between the rates of its transport into liver tissue from blood and its loss from liver tissue either by transport back to the blood or by uptake to Kupffer cells. The ratio dCM/dt equals the rate of uptake and trapping of iron oxide agent by Kupffer cells. These two relationships can be described by the following equations, respectively:

$$dCe/dt = k_1Cp + k_2Ce + k_3Ce \quad (2)$$

$$dCm/dt = k_3Ce \quad (3)$$

Equations (2) and (3) can, therefore, be integrated and solved for Ce and Cm as a function of time, respectively, as follows:

$$Ce(T) = k_1 e^{-(k_2+K_3)T} \int_0^T Cp \cdot e^{(k_2+k_3)t} dt \quad (4)$$

$$Cm(t) = k_1 k_2 \int_0^t [e^{-(k_2+k_3)T} \int_0^T Cp \cdot e^{(k_2+k_3)t} dt] dT \quad (5)$$

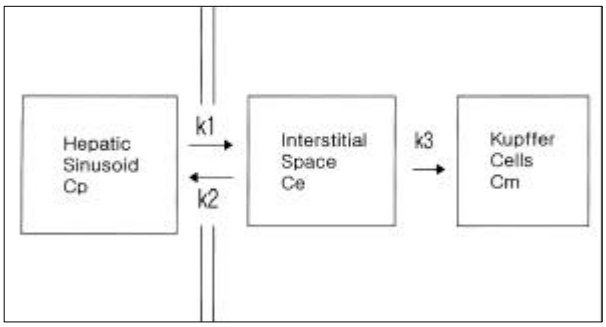

Fig. 1. Three-compartment model describing iron oxide nanoparticle kinetics. Cp=hepatic sinusoidal concentration; Ce=iron oxide concentration in the interstitial space; Cm=iron oxide concentration in Kupffer cells.

Pathologic studies

AMI-25 at 100 μmol/kg was injected in two New Zealand White rabbits (0.7 kg and 1.0 kg). Eighteen hours after injection, the rabbits were intraperitoneally anesthetized with 1g/kg of ethyl carbamate and the liver tissue was obtained. Histologic examination was performed with H & E and Prussian blue stain for iron detection. Micrographs were obtained at 5,000 - 50,000 × magnification using Transmission electron microscope (Hitachi H-600, Tokyo, Japan) at a 75 KV accelerating voltage.

Experiment with New Zealand white rabbits

We could not measure the signal intensity because of the small sizes of the aorta and portal vein. Being unable to achieve the arterial input, which is necessary for the quantification of variables among the three compartments, we instead adopted the kidney, which has non-specific uptake because of the lack of active phagocytic cells.

The three compartmental model of the liver includes plasma (Cp, Vp), extracellular interstitial space (Ce, Ve) and the intracellular space of Kupffer cells (Cm, Vm) (Fig. 1), whereas the kidney is represented by a two compartmental model that includes only plasma and extracellular interstitial space. We assumed that the distribution volume Ve is identical in the liver and kidney, and that AMI-25 enters a condition of steady state. It was suggested that the concentration of contrast material is linearly related to $\triangle R_2$ in an MR study.[9]

$$\triangle R_2(t) = -\ln[S(t)/S(0)]/T_E \quad (6)$$

The regional $\triangle R_2$ time curves after bolus injection of AMI-25 can be used for graphic analysis instead of the concentration curves in equation 4:

$$\frac{\int_0^t C_{Liv}(t)dt}{C_{Liv}(t)} = a \bullet \frac{\int_0^t fC_a(t)dt}{C_{Liv}(t)} + b \quad (7)$$

and

$$\frac{\int_0^t C_{Kid}(t)dt}{C_{Kid}(t)} = a' \bullet \frac{\int_0^t fC_a(t)dt}{C_{Kid}(t)} + b' \quad (8)$$

for times during which the transport of iron oxide from the extracellular interstitial space (Ve) to the intracellular space of Kupffer cells (Vm) is unidirectional, where a, a′, b and b′ are constants. Combining Equations (7) and (8) after eliminating fCa(t)dt we obtain:

$$\frac{\int_0^t C_{Liv}(t)dt}{C_{Liv}(t)} = \frac{a}{a'} \bullet \frac{\int_0^t C_{Kid}(t)dt}{C_{Liv}(t)} + (\frac{ab'}{a'}) \bullet \frac{C_{Kid}(t)}{C_{Liv}(t)} + b \quad (9)$$

The partial regression coefficients of equation 9 (a/a′, ab′/a′, b) can be acquired by multiple regression analysis. The coefficient a/a′ is related to equilibrium distribution volume and Rv can be obtained from the coefficient a/a′ (equation 10).

$$Rv = Vm/Ve = a/a' - 1 \quad (10)$$

Rv is defined as ratio of distribution volume (Vm/Ve), which is a measure of relative phagocytic activity.

Quantification of phagocytosis

For selective blockage of the reticulo-endothelial system, twelve New Zealand white rabbits (2.2 ± 0.8 kg) were randomly allocated to receive intravenously either: 2 ml of normal saline/kg (n=6); or 50 mg Si (silica suspension, 1-5 μm, Sigma) in 2 ml of normal saline/kg (n=6). MR study and radioisotope study were performed at 12 - 15 hours after the injection.[16-19] The rabbits were intraperitoneally anesthetized with 1g/kg ethyl carbamate in both studies.

MRI studies were performed using a 1.5T Signa (GE Medical System, Milwaukee, Wisconsin, USA). Axial slices of 4-mm thickness were taken simultaneously at the liver and kidney. A dynamic enhanced MRI time series were acquired with double slice spin echo planar sequence (TR/TE=3000/25 msec, pixel size=1.36 mm, temporal resolution=3 sec). A bolus of AMI-25 (20 μmol/kg) was injected after acquisition of ten phases. Total acquisition time for the series was 50 minutes.

Radioisotope study using Tc^{-99m}-phytate was used as the gold standard to represent active phagocytic Kupffer cells in the liver. An infusion of 0.3 - 0.4 mCi/kg of Tc^{-99m}-phytate was made over 10 seconds via an ear vein. $T_{1/2}$ was derived from the plasma clearance curve obtained from the blood samples every 1 minute for the first 10 minutes and then every 5 minutes for 45 minutes. After a further 45 minutes, the liver was extracted

and thoroughly homogenized. The radioactivity of homogenized tissue samples was also measured.

Steady state and the effect of injecting different doses of AMI-25

New Zealand white rabbits (2.0 ± 0.5 kg) were randomly allocated into three groups. Group 1 (n=3) underwent non-silica treatment and an AMI-25 60 μmol/kg bolus injection, group 2 (n=3) a non-silica treatment and an AMI-25 30 μmol/kg bolus injection, and group 3 (n=3) a silica treatment and an AMI-25 60 μmol/kg bolus injection. The rabbits were intravenously injected with either: 2 ml of normal saline/kg (groups 1 and 2); or 50 mg Si (silica suspension, 1 - 5 μm, Sigma) in 2 ml of normal saline/kg (group 3). Animals were intraperitoneally anesthetized by an injection of 1g/kg ethyl carbamate. MR studies were performed at 12 - 15 hours after the Si injection for group 3.

MR studies were performed in the same manner as described in experiment (1). A bolus of AMI-25 was injected after acquiring five phases. Total acquisition time of the series was over 80 minutes. Using dynamic AMI-25 enhanced MRI, the curve of $\triangle R_2$ versus time was plotted, the curve was then fitted and multiple regression analysis of the Rv time curve was performed using the Rv values obtained by the previously described equation 9.

Experiment with Beagle dogs

The limitation of the rabbit study was the lack of liver input function, which was supplied by the hepatic artery and portal vein. To estimate the transport rate between the biological compartments, the system input function is required. Therefore, Beagle dogs were used to measure the input function.

Five Beagle dogs (9.7 ± 1.64 kg) were anesthetized intravenously with ketamine HCl (5 - 10 mg/kg) and intubated and ventilated on O2 with enflurane (1 - 3%). Heart rate and degree of oxygen saturation were monitored continuously. For selective blockade of the reticulo-endothelial system, the animals were allocated to intravenously receive either: 5 ml of normal saline/kg for the control group (n=2): 100 mg/kg Si (silica suspension, 1 - 5 mm, Sigma) in 5 ml of normal saline/kg (n=1): or 350 mg/kg Si (n=2).

Dynamic liver imaging with Fast Gradient Echo Recalled At Steady State (TR/TE=11.1/4.2 msec, flip angle=20, pixel dimension=0.78 mm, slice thickness=5 mm, NEX=1, temporal resolution=2.6 sec) was performed using the breath-holding technique. The maximum breath-holding period was 90 seconds. The time schedule for image scanning was as follows: 5 pre-contrast images, 60 immediate post-contrast images, 60 further images after a 20 second break, 10 images every 10 minute for the first hour and then 10 images every 20 minute thereafter for up to three hours.

Data analysis

MR imaging data from the livers and kidneys of rabbits and from the livers, aortas and portal veins of Beagle dogs were directly transferred into a personal computer. Signal intensity was obtained from the MR images using Scion image software (version 4.02, Scion) requiring an ROI exceeding 200 pixels. Signal intensity transformed $\triangle R_2$ according to the equation: $\triangle R_2(t)=-\ln[S(t)/S(0)]/T_E$. A Levenberg-Marquardt optimizer fitting algorithm in Maltab software (version 5.1, Mathworks) was used to fit the $\triangle R_2$ time curve. In the rabbit experiment, Rv values were obtained from the fitted $\triangle R_2$ graph and the Rv time curve was obtained using Maltab software in a PC. In the experiment with beagle dogs, $\triangle R_2$ input was obtained from the signal intensities of the aorta and portal vein. The transport rate was then calculated in the three-compartment model using Maltab software in a PC.

RESULTS

Histologic findings

Photomicrography of H & E stained sections showed no abnormal pigment in the Kupffer cells or hepatocytes. Prussian blue staining showed blue pigment in the Kupffer cells, which specifically demonstrated the presence of deposited iron Kupffer cells (Fig. 2A). Electron micrography at 5,000 × showed multiple small granules in the

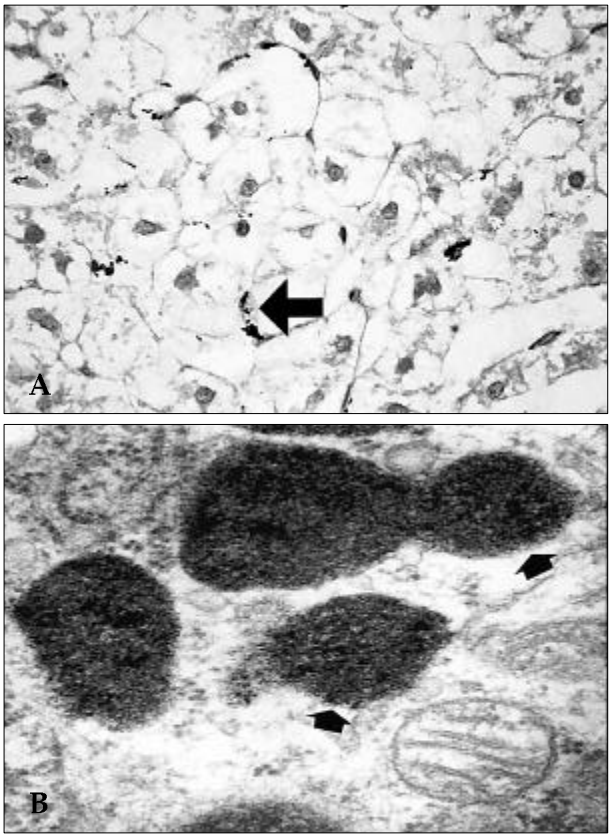

Fig. 2. Photomicrograph (Prussian blue stain ×200) (A) and a transmission electron micrograph (×50000) of the liver (B). A. Stainable iron is observed as pigment in the Kupffer cells (arrowed) B. The electron micrograph shows aggregation of AMI-25 particles in the lysosome (arrowed).

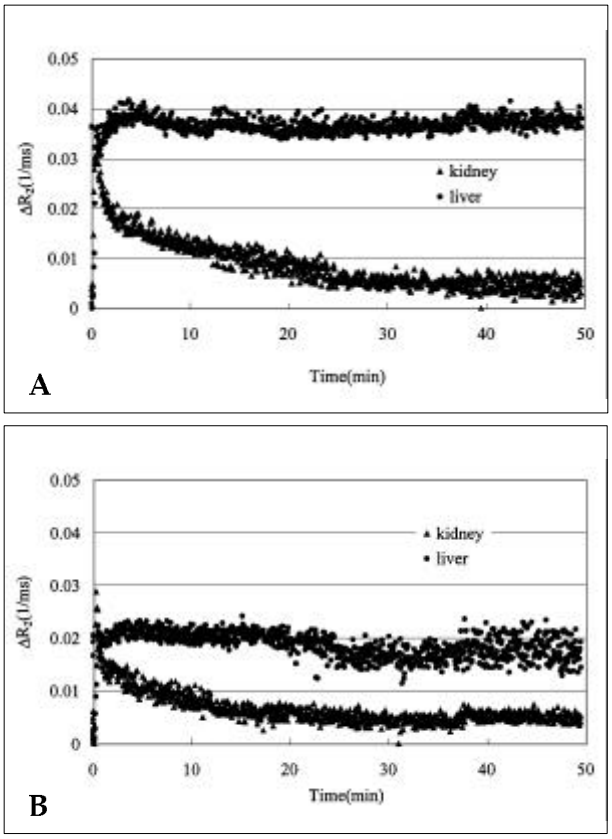

Fig. 3. $\triangle R_2$ of the liver and kidney as a function of time in normal (A) and the silica treated group (B). $\triangle R_2$ of the liver is twice as high in the normal group than in the silica treated group within 5 minutes after the injection of superparamagnetic iron oxide nanoparticles, but the $\triangle R_2$'s of the kidney for these two groups are similar.

cytoplasm of Kupffer cells. Aggregation of AMI-25 particles was observed in lysosomes at 50,000× (Fig. 2B).

Experiments with New Zealand white rabbits

In the first experiment, $\triangle R_2$ of the liver as a function of time was 0.04 (1/msec) in the normal group and 0.02 (1/msec) in the silica treated group within 5 minutes after bolus injection, but $\triangle R_2$ of the kidney was similar in the two groups (Fig. 3). After multiple regression analysis of the graphical analysis results, Rv was 6.42 ± 0.35 in the normal group and 2.98 ± 0.16 in the silica treated group. Tissue counts were 15,586 ± 1,226 (cpm/mCi/g) in the normal group and 10,130 ± 4,031 (cpm/mCi/g) in the silica treated group. $T_{1/2}$ (min) was more prolonged in the silica treated group (2.95 ± 0.17 minutes) than in the normal group (1.63 ± 0.32 minutes).

In the second experiment, the Rv time curve demonstrated that Rv approached a stable value 80 minutes after AMI-25 bolus injection in the liver of groups 1 and 2 (Fig. 4A). In group 3 (silica treated group), the Rv continued to increase at the end of the examination and a stable Rv value was unobtainable (Fig. 4B). The Rv values at 80 minutes after AMI-25 bolus injection were 5.06 in group 1, 6.20 in group 2 and 2.13 in group 3 (Table 1). The Rv values did not change with variations in AMI-25 injection dosage. The decrease in Rv value of the silica treated group corresponded to damage to active phagocytic Kupffer cells.

Experiment with Beagles

In the case of the Beagles, the input function

Table 1. Rv Values of the Three Different Groups 80 Minutes after AMI-25 Bolus Injection

Iron oxide	60 μmol/kg	30 μmol/kg	60 μmol/kg silica-treated
Rv (80 min)	6.83	6.04	3.51
	4.19	6.66	1.54
	4.16	5.89	1.35
Mean	5.06 ± 1.53	6.02 ± .41	2.13 ± 1.20

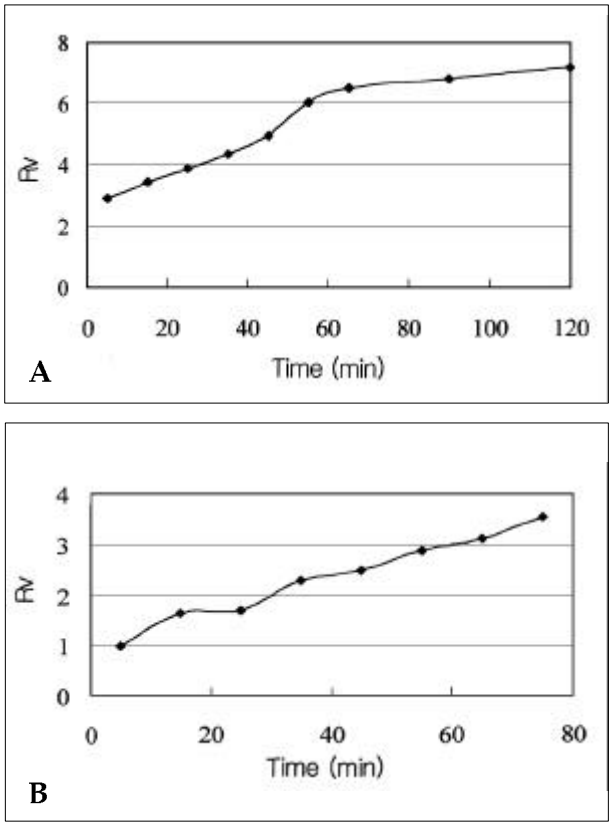

Fig. 4. Rv as a function of time following 60 μmol/kg AMI-25 bolus injection in normal (A) and silica treated rabbits (B). Rv reaches a maximum value at ca. 80 minutes after the AMI-25 injection, and then maintains this level until 120 minutes in normal group. But, Rv in silica treated group continued to increase until 120 minutes.

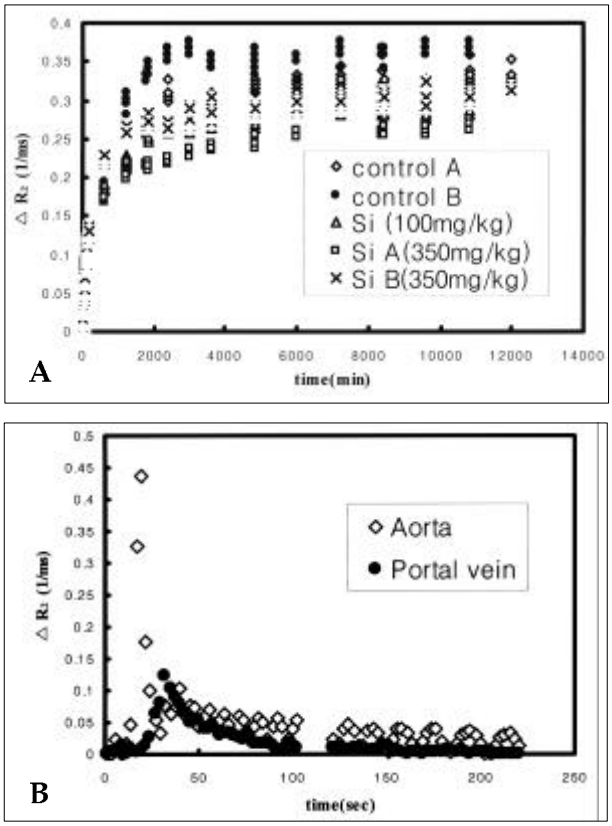

Fig. 5. $\triangle R_2$ of the liver as a function of time (A), and $\triangle R_2$ of the hepatic artery and portal vein as a function of time less than 3 minute in Silica treated case at a dose of 350 mg/kg (Si B) (B). $\triangle R_2$ of the normal and silica treated groups continued to increase for 3 hours, when the last measurements were obtained. $\triangle R_2$ of the hepatic artery and portal vein were measurable, but $\triangle R_2$ became too low to be traced within 3 minutes after the injection of superparamagnetic iron oxide nanoparticles.

could be represented by the measurement of $\triangle R_2$ in the aorta and portal vein (Fig. 5A). $\triangle R_2$ values in the blood and liver as a function of time are displayed in Fig 5B. $\triangle R_2$ in liver tissue appeared to increase continuously, at variable rate, for up to 3 hours, whereas $\triangle R_2$ differed in the control and silica treated groups. The rate of the transport constants, k1, k2, and k3, could not be estimated using the three compartment model.

DISCUSSION

The reticulo-endothelial system consists of organ macrophages, and macrophages in the liver and spleen account for 85% to 95% of the total intravascular phagocytic activity. Moreover, the

phagocytic activity of Kupffer cells is more extensive than that of the spleen.[20]

Ingested matters in the phagosome of the cytoplasm and the fusing of a phagosome with a lysosome allows the degradation of ingested matters by hydrolytic enzymes. Similarly, iron oxide nanoparticles are phagocytosed by Kupffer cells and the iron is modified in the lysosomes of Kupffer cells and incorporated into hemoglobin.[4] In our study, iron existed only in Kupffer cells by Prussian blue staining, and electron micrographs showed granules in the cytoplasms and aggregation of AMI-25 particles in lysosomes. Therefore, we confirmed that iron oxide nanoparticles are phagocytosed by Kupffer cell and are located in lysosomes.

The reticulo-endothelial system has a large phagocytic capacity and the "colloid clearance" method was developed for its measurement. In 1941, Maxfield and Mortensen investigated the measurement of phagocytic capacity in a quantitative manner using colloidal thorium dioxide,[21] while Halpern applied mathematical expressions and suggested the use of a clearance rate index, called the global phagocytic index (K), as a measure of physiologic phagocytic activity.[20] Dobson and Jones explained the specific nature of the colloidal disappearance curve and the selective localization of injected colloid in the liver and spleen, and emphasized the value of the critical colloid dose and the half time ($T_{1/2}$).[22] Biozzi et al. determined the relative liver and spleen sizes and developed the concept of the "corrected phagocytic index" (α), as a comparative index of reticulo-endothelial functional activity between species.[23] The quantification of phagocytic activity was further developed and radio-colloid used clinically for liver imaging. We used radio-colloid as a gold standard and examined the use of Tc^{99m}-phytate, which is mainly distributed in the liver.[24] In the present study, in silica treated rabbits radioactivity was reduced by 65% and the $T_{1/2}$ derived from the plasma clearance curve prolonged by 180% compared to the normal rabbit.

It is well known that silica effectively blocks the reticulo-endothelial system of variable mammals.[16-19] However, the saturation effect of the reticulo-endothelial system differs between rabbits and dogs, and the latter becomes saturated at larger doses.[18,19] Thus, in the present study, the silica dose used for the dogs was sevenfold that used for the rabbits.

We used the three-compartment model in iron oxide nanoparticle phagocytic modeling, whereas the models most frequently applied are two and three compartment models. The two compartment model has plasma and tissue compartments and the three compartment model contains plasma, interstitial and cellular compartments.[12,13] It is well known that iron oxide nanoparticles are transported from plasma to the interstitial space of the liver and phagocytosed by Kupffer cells. In the Kupffer cell, iron exists for a long time before degradation. In experiments with rats, $\triangle R_2$ of AMI-25 increased for 4 hours, and the $T_{1/2}$ of the liver signal intensity was 24 - 48 hours.[4] In pharmacokinetic modeling, a model should represent the characteristic metabolic pathway of a certain material. Therefore, the three-compartment model should represent the characteristic metabolism of iron oxide nanoparticles.

Iron oxide nanoparticles, a negative contrast agent, increase the relaxation rate, which shortens T2 and lowers the signal intensity. Iron oxide nanoparticles also increased spin-lattice relaxation, R1, which further shortens T1. However, T1 shortening was minimal compared to T2 shortening. Majumdar et al. reported a relaxation rate of 1.4 ± 0.3 sec-1/mg(iron)/g(liver) for T1, and 93.4 ± 4.4 sec-1/mg(iron)/g(liver) for T2 in rat.[2] Therefore we usually determine the transverse relaxation rate, R_2. We obtained $\triangle R_2$ from the liver signal intensity and determined the transport rate using the $\triangle R_2$ time curve.

Several non-invasive methods are used to measure k3/k4 in the three-compartment model; the peak equilibrium ratio (R_{PE}) method, the ratio of distribution volumes (R_v) method, and the area ratio (R_A) method.[13] These methods do not need arterial blood sampling for the input function. Unlike R_{PE} or R_A, R_v is not affected by regional blood flow or clearance. R_v should theoretically be the same as that obtained by the original graphic method using appropriate arterial input function.[13] In our rabbit experiment, we used the concept of Rv value. As the input function could not be measured because of the small aorta and portal vein, we adopted a method for eliminating the

influence of the arterial input function by simultaneously imaging and acquiring data of the kidney and liver. We suggest that R_v represents phagocytic activity, and we determined the R_v in rabbits, which showed decreased phagocytic activity following silica injection. The R_v decreased in the silica treated group as it was also found to do in a radioisotope study with Tc^{-99m}-phytate and $T_{1/2}$. Therefore, it was concluded that R_v represents decreased phagocytic activity in the liver. R_v reached a steady state 80 minutes after iron oxide dosing and did not change iron dosage.

In mammals, the input function of the liver is comprised of the supplies by the portal vein (80%) and the hepatic artery (20%).[25] We assumed that the concentration of iron oxide in the hepatic artery blood is equal to that of the aorta. Therefore, the concentration of iron oxide nanoparticles in liver tissue is the sum of the concentration of iron oxide delivered by the portal vein and the aorta. But the rate transport constant could not be estimated. Our results suggest several possible causes. Firstly, the transport rate is species dependent. The liver $\triangle R_2$ in the Beagle increased continually over the 3 hour period of measurement without plateauing. However, in the rabbit a plateau formed within 80 minutes. Because the iron oxide nanoparticles did not reach steady state in case of Beagle dogs, the system did not obey first order kinetics. Hence, the transport rate varied and could not be estimated.

Secondly, the transverse relaxation change by iron oxide in the liver tissue may not be the same in vessels such as aorta and portal vein, because distributional differences. Tanimoto reported a T2-relaxation rate reduction in Sephadex phantoms compared to agar phantoms (the Sephadex phantom had a heterogeneous spatial distribution).[26] This suggests that the T2 relaxation effect of iron oxide depends on spatial resolution. Phantoms with Sephadex beads simulate iron oxide distribution in the liver, whereas without Sephadex beads the phantoms resemble the spleen. Phantoms without Sephadex beads showed linear increases of R_1 and R_2 with increasing iron oxide concentration; however, with Sephadex beads R_1 and R_2 showed little change.[3] This results suggests that the signal intensities of different organs may differ at the same iron oxide concentration. Weissleder, et al. investigated the pharmacokinetics of iron oxide using a ^{59}Fe radiotracer.[4] They measure the bio-distribution of AMI-25 by using ^{59}Fe and by relaxation time studies, and found it to be consistent with a model of initial vascular distribution and specific uptake in reticulo-endothelial cells. After iron was degraded in lysosomes, the bio-distribution of AMI-25, as measured using ^{59}Fe, differed from that observed in relaxation time studies.

Thirdly, it is difficult to measure input functioning. We obtained an $\triangle R_2$ measurement in the aorta and portal vein. Within 3 minutes, the $\triangle R_2$ value of the input function had become very small, which may have produced the significant source of noise in the curve estimation of arterial input function.

In conclusion, Rv (Vm/Ve) may be a quantitative index of reduced phagocytic activity in the liver by dynamic iron oxide enhanced MRI.

REFERENCES

1. Majumdar S, Zoghbi S, Pope CF, Gore JC. A quantitative study of relaxation rate enhancement produced by iron oxide particles in polyacrylamide gels and tissue. Magn Reson Med 1989;9:185-202.
2. Majumdar S, Zoghbi S, Pope CE, Gore JC. Quantitation of MR relaxation effects of iron oxide particles in liver and spleen. Radiology 1988;169:653-5.
3. Tanimoto A, Oshio K, Suematsu M, Pouliquen D, Stark DD. Relaxation effects of clustered particles. J Magn Reson Imaging 2001;14:72-7.
4. Weissleder R, Stark DD, Engelstad BL, Bacon BR, Compton CC, White DL, et al. Superparamagnetic iron oxide: pharmacokinetics and toxicity. AJR Am J Roentgenol 1989;152:167-73.
5. Kawamura Y, Endo K, Watanabe Y, Saga T, Nakai T, Hikita H, et al. Use of magnetic particles as a contrast agent for MR imaging of the liver. Radiology 1990;174: 357-60.
6. Thickman D, Hendrick RE, Jerjian KA, Schanker CS. Liver-lesion tissue contrast on MR imagies: effect of iron oxide concentration and magnetic field strength. Radiology 1990;176:557-62.
7. Hahn PF, Stark DD, Weissleder R, Elizondo G, Saini S, Ferrucci JT. Clinical application of superparamagnetic iron oxide to MR imaging of tissue perfusion in vascular liver tumors. Radiology 1990;174:361-6.
8. Oudkerk M, van den Heuvel AG, Wielopolski PA, Schmitz PIM, Borel Rinkes IHM, Wiggers T. Hepatic lesion: detection with ferumoxide enhanced T1-

weighted MR imaging. Radiology 1997;203:449-56.
9. Mandeville JB, Moore J, Chesler DA, Garrido L, Weissleder R, Weisskoff RM. Dynamic liver imaging with iron oxide agents: effects of size and biodistribution on contrast. Magn Reson Med 1997;37:885-90.
10. Jung CW, Jacobs P. Physical and chemical properties of superparamagnetic iron oxide MR contrast agents: ferumoxides, ferumoxtran, ferumoxsil. Magn Reson Imaging 1995;13:661-74.
11. Josephson L, Lewis J, Jacobs P, Hahn PF, Stark DD. The effects of iron oxides on proton relaxivity. Magn Reson Imaging 1988;6:647-53.
12. Sokoloff L, Reivich M, Kennedy C, Des Rosiers MH, Patlak CS, Pettigrew KD, et al. The [14C]Deoxyglucose method for the measurement of local cerebral glucose utilization: theory, procedure, and normal values in the conscious and anesthetized albino rat. J Neurochem 1977;28:897-916.
13. Ichise M, Ballinger JR, Golan H, Vines D, Luong A, Tsai S, et al. Nonivasive quantification of dopamine D2 receptors with iodine-123-IBF SPECT. J Nucl Med 1996;37:513-20.
14. Laruelle M, van Dyck C, Abi-Dargham A, Zea-Ponce Y, Zoghbi SS, Charney DS, et al. Compartmental modeling of iodine-123-iodobenzofuran binding to dopamine D2 receptors in healthy subjects. J Nucl Med 1994;35:743-54.
15. Pardridge WM, Crane PD, Mietus LJ, Oldendorf WH. Kinetics of regional blood brain barrier transport and brain phosphorylation of glucose and 2-deoxyglucose in the barbiturate-anesthetized rat. J Neurochem 1981; 38:560-8.
16. Souhami RL, Bradfield JW. The recovery of hepatic phagocytosis after blockage of Kupffer cells. J Reticuloendothel Soc 1974;16:75-86.
17. Friedman RL, Moon RJ. Hepatic clearance of Salmonella typhimurium in silica-treated mice. Infect Immun 1977;16:1005-12.
18. Albridge CM, Dudley HAF. Detection of reticulo-endothelial blockage with low-dose test agent. Br J E Pathol 1985;66:483-91.
19. Banaszak EF, Kampine JP, Brault BA, Smith JJ. Circulatory effects of RES depression in the dog. Am J Physiol 1965;209:532-8.
20. Saba TM. Physiology and physiopathology of the reticuloendothelial system. Arch Intern Med 1970;126:1031-52.
21. Maxfield FA, Mortensen OA. The use of the radioactive properties of thorium for a quantitative study of phagocytosis. J Appl Physics 1941;12:197-202.
22. Dobson EL, Jones HB. The behavior of intravenously injected particulate material. Acta Med Scand 1952;273: 1-71.
23. Biozzi G, Benacerraf B, Halpern BN. Quantitative study of the granulopectic activity of the reticuloendothelial system: a study of the kinetics of the granulopectic activity of the R.E.S in relation to the dose of carbon injected: relationship between the weight of the organs and their activity. Brit J E Pathol 1953;34:97-106.
24. Adams FG, Horton PW, Selim SM. Clinical comparison of three liver scanning agents. Eur J Nucl Med 1980;5: 237-9.
25. Pinakatt T, Richardson AW. Distribution of cardiac output in dogs. Am J Physiol 1967;213:905-9.
26. Tanimoto A, Pouliquen D, Kreft BP, Stark DD. Effects of spatial distribution on proton relaxation enhancement by particulate iron oxide. J Magn Reson Imaging 1994;4:653-7.